

## Multiple magnetic singlet-singlet excitations in intermetallic PrNiSn

K. A. McEwen,<sup>1</sup> J. Jensen,<sup>2</sup> E. D. Beirne,<sup>1</sup> J. P. Allen,<sup>1</sup> K. Habicht,<sup>3</sup> D. T. Adroja,<sup>4</sup> R. I. Bewley,<sup>4</sup> and D. Fort<sup>5</sup><sup>1</sup>Department of Physics and Astronomy, University College London, Gower Street, London WC1E 6BT, United Kingdom<sup>2</sup>Niels Bohr Institute, Universitetsparken 5, 2100 Copenhagen, Denmark<sup>3</sup>Berlin Neutron Scattering Centre, Hahn-Meitner-Institute, Glienicke Strasse 100, 14109 Berlin, Germany<sup>4</sup>ISIS Facility, Rutherford Appleton Laboratory, Chilton, Didcot OX11 0QX, United Kingdom<sup>5</sup>Department of Metallurgy and Materials, University of Birmingham, Edgbaston, Birmingham B15 2TT, United Kingdom

(Received 25 August 2005; revised manuscript received 9 November 2005; published 3 January 2006)

Inelastic neutron-scattering experiments have been carried out on a polycrystalline sample of PrNiSn, and seven of the eight excited crystal-field singlets of the Pr ions were detected. The system stays paramagnetic, at least down to 0.9 K, and the three principal susceptibility components have been measured on a PrNiSn single crystal between room temperature and 1.7 K. The crystal-field excitations of the single crystal at low temperatures have been studied by triple-axis neutron spectroscopy. Dispersive effects are observed for three different levels of singlet-singlet excitations. The results are analyzed in terms of a mean-field/random phase approximation model, and it is concluded that the exchange interaction is highly anisotropic and of long range. The critical ratio between the maximum of the exchange interaction and that required for inducing a magnetic ordering of the singlet ground-state system is derived to be 0.48, leading to a predicted ordering temperature of 6 mK for the combined electron-nuclear magnetic system.

DOI: 10.1103/PhysRevB.73.014402

PACS number(s): 75.20.En, 78.70.Nx, 75.10.Dg

## I. INTRODUCTION

PrNiSn is a member of the *RTX* series of intermetallic compounds. The rare-earth systems RNiSn cover a wide area within magnetism; CeNiSn and YbNiSn show Kondo phenomena,<sup>1,2</sup> and the heavy rare-earth Gd, Dy, Ho, and Er compounds order antiferromagnetically.<sup>3,4</sup> Of the light rare earths,<sup>5</sup> NdNiSn is found to order antiferromagnetically,<sup>6,7</sup> whereas heat capacity measurements<sup>6</sup> indicate that PrNiSn stays nonmagnetic down to 0.9 K. In comparison with the other RNiSn compounds, relatively little work has been done on the magnetic properties of PrNiSn. Here, we present inelastic neutron-scattering experiments and susceptibility measurements on PrNiSn: a preliminary account has been published in Ref. 8. The single-crystal susceptibility measurements and the neutron-scattering experiments on a polycrystalline sample have been used to derive the crystal-field (CF) Hamiltonian of PrNiSn, as presented in Sec. II. The experimental dispersion along symmetry directions of the three lowest crystal-field levels has been determined from single-crystal studies and is compared with the excitation spectrum derived from the CF Hamiltonian of Sec. II. The crystal structure of PrNiSn belongs to the same space group as HoF<sub>3</sub>, and the random phase approximation (RPA) theory applied in the present work is equivalent to the one developed previously for the case of HoF<sub>3</sub>.<sup>9-11</sup> These matters are discussed in Sec. III, and the conclusion is given in Sec. IV.

## II. CRYSTAL-FIELD HAMILTONIAN

The crystal structure of PrNiSn is the orthorhombic TiNiSi structure (space group number 62, *Pnma*) with the lattice parameters  $a=7.3848$  Å,  $b=4.5193$  Å, and  $c=7.5985$  Å (at 1.7 K). The Pr ions are located at the site 1,  $(x, \frac{1}{4}, z)$ ; site 2,  $(-x, \frac{3}{4}, -z)$ ; site 3,  $(\frac{1}{2}+x, \frac{1}{4}, \frac{1}{2}-z)$ ; and site 4,  $(\frac{1}{2}-x, \frac{3}{4},$

$\frac{1}{2}+z)$ ; where  $x=-0.0214$  and  $z=0.6967$ . The numbering of the sites from 1 to 4 defines the four different Pr sublattices. The projection of the unit cell on the *ac* plane is shown in Fig. 1.

The point symmetry at the Pr sites is low. The only symmetry element at these sites is the mirror plane perpendicular to the *b* axis. Assuming *x*, *y*, and *z* to be along the *a*, *b*, and *c* axes of the crystal, respectively, this symmetry element removes the Stevens' sine operators from the CF Hamiltonian of the Pr ions leaving 15 independent parameters:

$$\mathcal{H}_{\text{CF}} = \sum_{l=2,4,6} \sum_{m=0}^l B_l^m O_l^m(c). \quad (1)$$

The additional symmetry elements of the crystal imply that each of the parameters with *m* even are common for all four

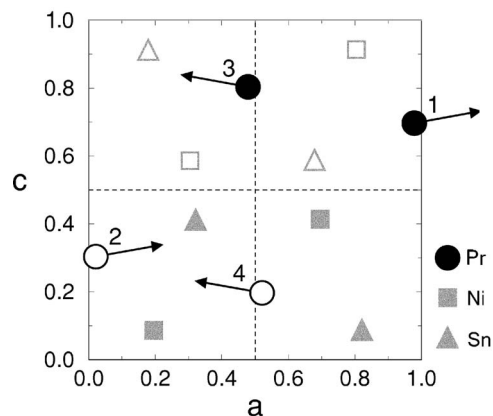


FIG. 1. The unit cell of PrNiSn projected onto the *ac* plane. The solid (open) symbols indicate the ions in the *ac* layer at  $b/4(3b/4)$ . The arrows indicate the direction of the ordered moments below a predicted  $T_N=6$  mK (see Sec. IV).

Pr sublattices, whereas the terms with  $m$  odd have opposite signs for the Pr ions belonging to the sublattices 3 and 4 and those belonging to the sublattices 1 and 2. The different signs of the odd- $m$  terms do not affect the positions of the crystal-field levels, and because of the low symmetry the  $J=4$  ground-state multiplet of the  $\text{Pr}^{3+}$  ions is expected to split up into nine singlets.

The crystal-field excitations in  $\text{PrNiSn}$  were first studied by inelastic neutron scattering on a polycrystalline sample. The sample was prepared by arc melting the constituent elements under an argon atmosphere. The purity was 99.999% for Ni and Sn and 99.9% for Pr. The mixture was melted several times to achieve homogeneity with a small percentage ( $<1\%$ ) of extra Sn to account for any mass loss. The neutron-scattering experiments were carried out on a 20 g  $\text{PrNiSn}$  polycrystalline sample on the HET chopper spectrometer at the ISIS Facility, United Kingdom. The sample was crushed and wrapped in an aluminum sachet with a face approximately  $4 \times 4 \text{ cm}^2$ . Inelastic measurements were taken at four different incident energies: 23, 35, 60, and 800 meV. Neutrons are scattered from the sample into two forward detector banks, one covering scattering angles from  $2.6^\circ$  to  $7.2^\circ$  at a distance of 4 m from the sample position, and a second bank covering scattering angles from  $9.3^\circ$  to  $28.7^\circ$  at a distance of 2.5 m from the sample. Two detector banks located at high scattering angles ( $110.4^\circ$ – $138.7^\circ$ ) are valuable for the measurement of the phonon density of states. For a chopper spectrometer operating at a fixed incident neutron energy, the wave vector transfer is a function of the neutron energy transfer, as well as scattering angle. In the case of HET, for an incident neutron energy of  $E_i=35 \text{ meV}$ , the wave vector transfer at the mean scattering angle ( $\phi = 19.0^\circ$ ) of the 2.5 m detector bank is  $Q=1.36 \text{ \AA}^{-1}$  at zero energy transfer ( $E=0$ ),  $1.63 \text{ \AA}^{-1}$  at  $E=17 \text{ meV}$ , and  $2.34 \text{ \AA}^{-1}$  at  $E=27 \text{ meV}$ . For  $E_i=23 \text{ meV}$ , the corresponding figures are  $Q=1.10 \text{ \AA}^{-1}$  at  $E=0$ , and  $1.81 \text{ \AA}^{-1}$  at  $E=17 \text{ meV}$ . The data sets were normalized to the incoherent scattering from a vanadium standard sample for each incident energy. Second, the scattering data were corrected for the contributions due to the phonons leaving only the magnetic part of the scattering. For this purpose high-angle scattering data of the nonmagnetic reference compound  $\text{LaNiSn}$  were used. The magnetic scattering results obtained in this way at 10 K at the incident energies of 23 and 35 meV are shown in Fig. 2. We may add that the subtraction of the phonon contributions is of minor importance, e.g., the contribution is almost negligible in the inelastic, low-energy part of the spectrum obtained for  $E_i=23 \text{ meV}$ . The elastic cross section left after the correction has been performed is not an intrinsic magnetic response, but is due to incoherent scattering from the component atoms in the sample. When combining the two different results shown in Fig. 2 we identify seven of the possible eight excited crystal-field levels. Fitting the data with weighted Gaussians (these fits are not included in the figures) the energies of the levels were determined to be  $1.78 \pm 0.02$ ,  $3.33 \pm 0.02$ ,  $5.38 \pm 0.03$ ,  $7.34 \pm 0.14$ ,  $17.17 \pm 0.02$ ,  $23.49 \pm 0.07$ , and  $28.34 \pm 0.07$  in units of meV.

The susceptibility of polycrystalline  $\text{PrNiSn}$  has been previously determined by Routsis *et al.*<sup>5</sup> Here we report the results of measurements, using a PPMS9 Quantum Design

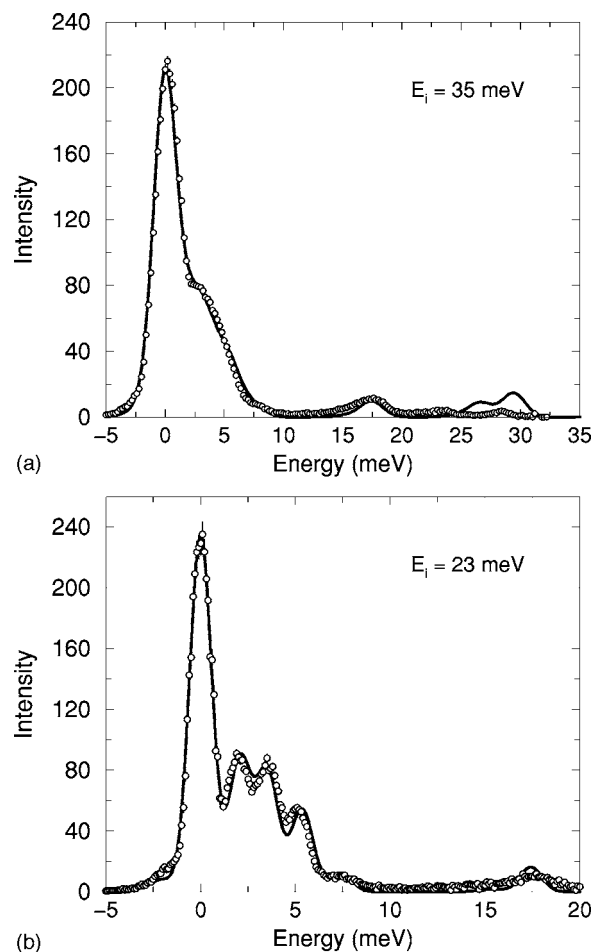


FIG. 2. The magnetic part of the neutron-scattering intensities at 10 K determined from polycrystalline  $\text{PrNiSn}$ , using the HET spectrometer, with an incident neutron energy  $E_i=35$  or  $23 \text{ meV}$ . In the lower figure the experimental data have been rigidly shifted  $0.1 \text{ meV}$  up in energy in order to center the elastic peak at zero energy. The solid lines are the final fits determined by the model CF Hamiltonian.

magnetometer, of the susceptibility along the three principal axes of a single crystal of  $\text{PrNiSn}$ . These results, from measurements in a magnetic field of  $0.03 \text{ T}$ , are shown in Fig. 3. The susceptibility is strongly anisotropic at  $T=2 \text{ K}$ , with  $\chi_{aa} \sim 1.5\chi_{bb}$ , and  $\sim 4\chi_{cc}$ . With increasing temperature,  $\chi_{aa}$  drops rapidly, and above  $14 \text{ K}$ , the  $a$ - $b$  anisotropy is reversed, so that  $\chi_{bb} > \chi_{aa}$  above this crossover temperature.  $\chi_{bb}$  has a clear local maximum around  $12 \text{ K}$  and a local minimum around  $4 \text{ K}$ . All of the susceptibility components show a distinct upturn below  $3 \text{ K}$ . However, this upturn became less apparent in higher fields, and was not observed above  $2 \text{ T}$ . The origin of this feature will be discussed below.

The scattering resulting from a polycrystalline sample is an average of the single-crystal response over all directions of the scattering vector. To a first approximation in the low-temperature limit, the dispersive effects are averaged out, leading to a response close to that produced by the isolated ions. The single-crystal susceptibility components and the inelastic neutron-scattering results from polycrystalline  $\text{PrNiSn}$  were calculated using the 15 CF parameters defined

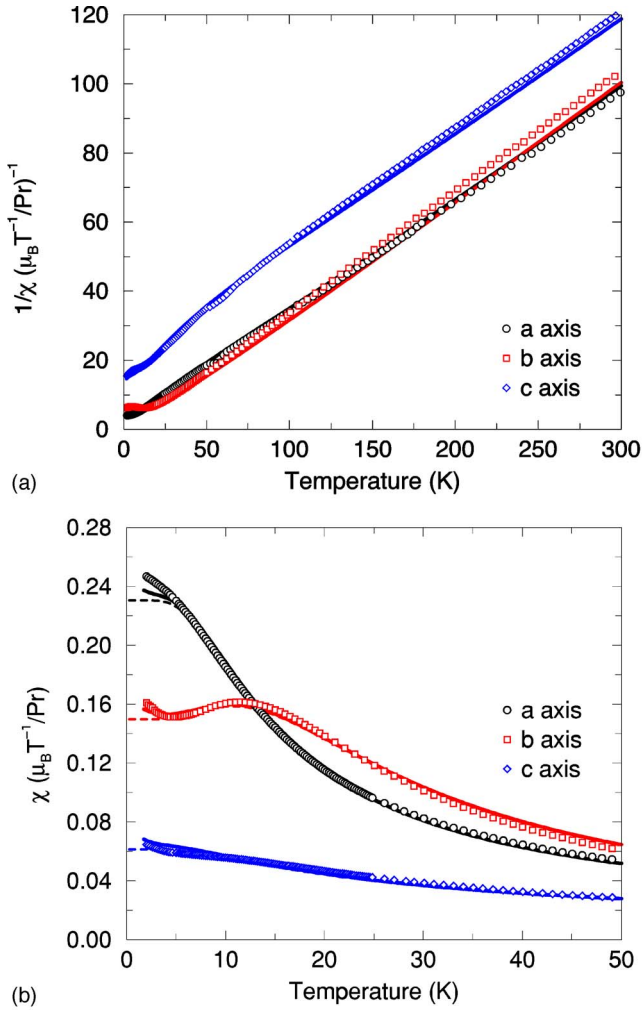


FIG. 3. (Color online) The inverse susceptibility components of PrNiSn are shown in (a). (b) Shows the susceptibility components at low temperatures. The solid lines are the calculated results when including the estimated contributions from paramagnetic impurities, whereas the thin dashed lines are the susceptibility components of the pure system.

by Eq. (1) as fitting parameters.<sup>12</sup> In addition, in the case of the neutron scattering results, we have  $2 \times 3$  more, an intensity scale parameter, a (constant) Gaussian linewidth, and an elastic cross section. With so many fitting parameters, it is unlikely that the experimental data will determine a unique set of CF parameters. However, this deficiency is unimportant for the practical consequences of our model. The key ingredients are the energies and the corresponding wave functions of the 4–5 lowest levels, or rather the different matrix elements of the angular-momentum operators between the lower levels. A least-squares procedure was developed for fitting all the above data simultaneously. It turned out to be difficult to obtain a reasonable description of the low-temperature behavior of the susceptibility components, especially to generate the maximum in the  $bb$  component at about 12 K. These difficulties actually mean that the multiplicity of choices for the 15 CF parameters is smaller than one may think initially. The analysis of the susceptibility data showed that it is important to include the effects of the two-

TABLE I. The crystal-field parameters of the Pr ions belonging to either the sublattices 1 and 2 or the sublattices 3 and 4 (in units of meV). The parameters  $B_l^m$  apply for all Pr ions, when  $m$  is even, but have opposite signs on the two sets of sublattices if  $m$  is odd.

$B_2^0$	0.1763	$B_6^0$	$-0.089 \times 10^{-3}$
$B_2^1$	-0.3342	$B_6^1$	$2.112 \times 10^{-3}$
$B_2^2$	-0.1413	$B_6^2$	$-0.460 \times 10^{-3}$
$B_4^0$	$-0.6663 \times 10^{-2}$	$B_6^3$	$2.308 \times 10^{-3}$
$B_4^1$	$0.5074 \times 10^{-2}$	$B_6^4$	$-1.051 \times 10^{-3}$
$B_4^2$	$-2.243 \times 10^{-2}$	$B_6^5$	$7.800 \times 10^{-3}$
$B_4^3$	0	$B_6^6$	$-2.824 \times 10^{-3}$
$B_4^4$	$3.724 \times 10^{-2}$		

ion interactions at zero wave vector. These exchange constants are anisotropic and in the final fit we use

$$\mathcal{J}_{xx}(\mathbf{0}) = \mathcal{J}_{zz}(\mathbf{0}) = 0.023 \text{ meV}, \quad \mathcal{J}_{yy}(\mathbf{0}) = 0.113 \text{ meV}. \quad (2)$$

The final values of the CF parameters are given in Table I and the corresponding calculated results are included in Figs. 2 and 3. In these calculations of the bulk susceptibilities and of the averaged, single-ion-like scattering intensities from the polycrystalline sample, it is not necessary to account for the difference in signs of the  $m$ -odd parameters between the sublattices (1,2) and (3,4). This also means that it is not possible to decide whether the choice of signs for the terms with odd  $m$  in Table I applies to the sublattices (1,2) or (3,4). That would require a determination of the easy axis within the  $xz$  plane for one of the sublattices, compare with the discussion of the HoF<sub>3</sub> system in Ref. 9. We should add that the magnetic excitation spectrum, calculated in the next section, is also independent of this choice between the sublattices (1,2) or (3,4), as long as  $\mathcal{J}_{xz}(ij)$  is negligible. At the lowest temperatures, where only the ground state of the CF system is populated, the susceptibility components should saturate. The experimental data, however, show upturns at the lowest temperatures in the case of all three components, which we attribute to an isotropic paramagnetic impurity signal,  $\Delta\chi = A/T$ , where we have used  $A = 0.012 \text{ K } \mu_B T^{-1}/\text{Pr}$ . This would correspond, for example, to a free Pr impurity concentration of about 0.4% in the sample. The comparison between experiments and theory in Figs. 2 and 3 is satisfactory except that the calculated high-temperature slope of the inverse  $bb$  susceptibility is slightly too small, and that the intensities and positions of the two highest levels, above 20 meV, in Fig. 2 differ somewhat. However, these discrepancies should not be significant for the excitations at the lower energies, which we discuss in the next section.

### III. MAGNETIC EXCITATIONS

From the HET data it is clear there are several low-lying crystal-field states below 10 meV. In order to study the dispersion of these excitations we have performed inelastic neutron-scattering experiments on a single crystal of PrNiSn.

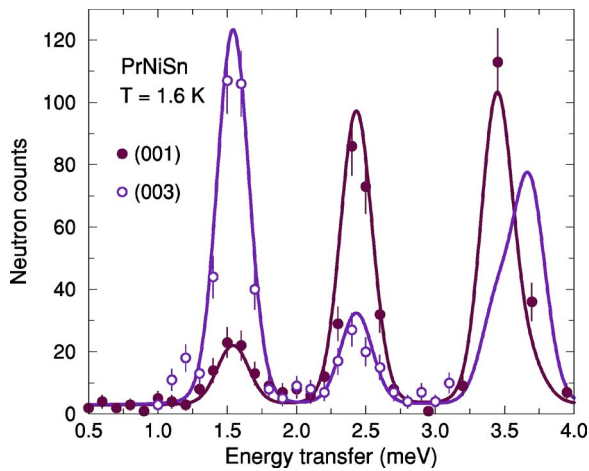


FIG. 4. (Color online) Inelastic neutron scans at (001) and (003) obtained at 1.6 K. The solid lines are the calculated results, where the resolution widths and intensity scales are assumed to be the same in the two scans.

The single crystal (4 g) was cut from an ingot grown by the Czochralski tri-arc technique, at the University of Birmingham. The experiments were carried out using the cold neutron triple-axis spectrometer V2 at the Berlin Neutron Scattering Center. The sample was mounted, in an Orange cryostat, with its  $b$  axis vertical. Measurements were made in the  $a^*c^*$  horizontal scattering plane, mostly with the spectrometer operated with fixed final wave vector  $k_f = 1.55 \text{ \AA}^{-1}$  and  $40'-60'-60'$  collimation. In this configuration, the experimental resolution (vanadium full width at half maximum) was 0.20 meV at zero energy transfer. One example is presented in Fig. 4, and it indicates the presence of (at least) three excitation branches below 4 meV. Scans along  $(q00)$  (see Fig. 5) show that there are actually two branches around 3.5 meV. There is also an additional one at the higher energies of about 5.2 meV. The latter mode is not visible in

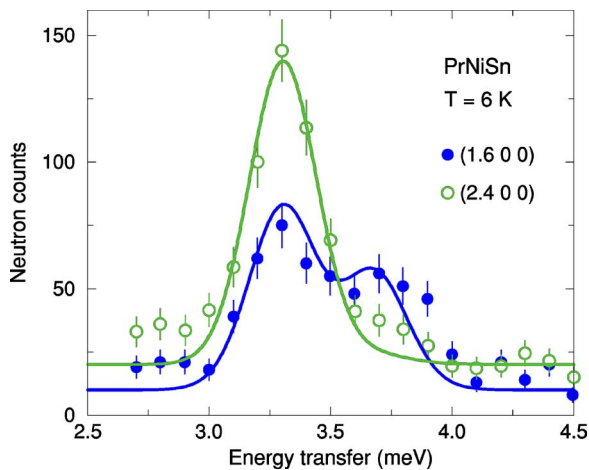


FIG. 5. (Color online) Inelastic neutron scans at (1.6 0 0) and (2.4 0 0) obtained at 6 K showing the  $yy$  excitations. The solid lines are the calculated results, when assuming that the resolution widths and intensity scales are the same in the two scans.

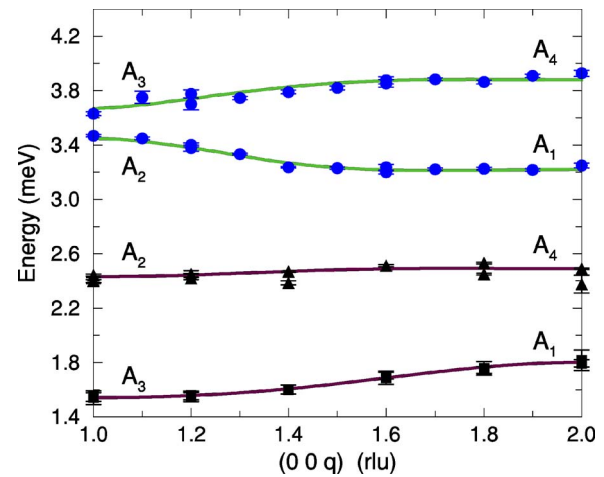


FIG. 6. (Color online) The dispersion relation along the  $c^*$  axis. The experimental results are indicated by the symbols. Some of these results were determined with  $q$  lying between 2 and 3 and have been mapped into the interval shown. The experimental results were determined at 6 and 1.8 K for the two upper and two lower branches, respectively. The solid lines are the corresponding calculated results.

$(00q)$  scans such as those shown in Fig. 4. The dispersion of all these excitations has been measured both along  $c^*$  and  $a^*$ , and the results are shown in Figs. 6 and 7. The neutron scans at some of the  $q$  values along  $(q00)$  in Fig. 7 indicate the presence of more than the expected two peaks at energies close to 3.5 meV. The results for the excitation energies at these  $q$  values depend somewhat on whether the extra peaks

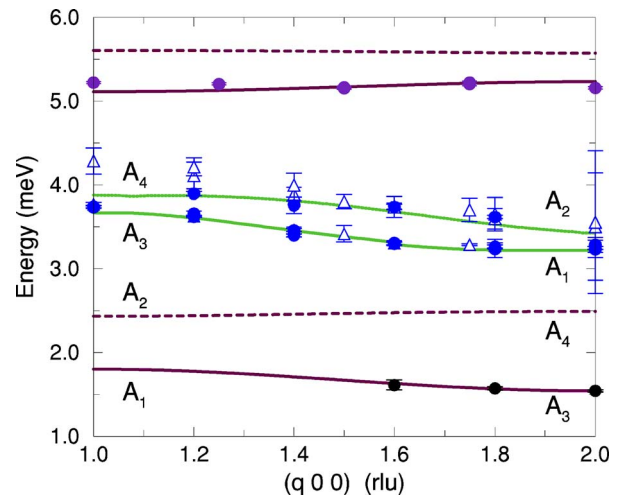


FIG. 7. (Color online) The dispersion relation along the  $a^*$  axis. The measurements were performed at the same temperatures (6 K and 1.8 K), and as in the case of Fig. 6, some of the experimental results were obtained for  $q$  between 2 and 3. The three experimental results for the lowest branch were measured at  $(2-q01)$ . Some of the experimental results obtained for the branches lying between 3 and 4 meV are represented by two different symbols, which are the results of two different Gaussian fits to the same neutron-scattering data. The lines show the calculated dispersion relations with the dashed ones indicating low-intensity branches.

TABLE II. The three lowest excitation energies ( $\Delta$ ) and the squared matrix elements of the angular-momentum components between the ground state and the excited levels, as predicted by the crystal-field Hamiltonian.

$\Delta$ (meV)	$ M_x ^2$	$ M_y ^2$	$ M_z ^2$
2.068	5.4215	0	0.1594
3.535	0	4.5775	0
5.368	0.1019	0	2.8861

are included in the Gaussian fits or not, as indicated on the figure. One likely possibility is that the additional small peaks are due to a low-lying phonon branch.

The RPA method used for calculating the excitation spectrum in the paramagnetic phase of PrNiSn is the same as was used in the case of HoF<sub>3</sub> (see Refs. 9–12). Both compounds belong to the space group *Pnma*. However, there are some differences. In the PrNiSn system, the hyperfine interaction is unimportant (above 10 mK), and the classical dipole-dipole interaction is relatively weak compared with the exchange interaction (a factor of 100 smaller). These two complications may therefore be safely neglected in PrNiSn. The crystal-field Hamiltonian predicts the level scheme given in Table II for the lowest levels. This table shows that the lowest excitation mode is polarized almost completely along the *x* axis, whereas the second level gives rise to excitations polarized parallel to the *y* axis, and the third mode is polarized nearly along the *z* axis. This classification accords with the observed polarization dependence of the cross sections. The two lowest branches are observed along (0 0 *q*), but not along (*q* 0 0), whereas the opposite applies to the uppermost level. The *yy*-polarized excitations are observed in both types of scans. The presence of four Pr ions per unit cell implies that each of the three levels gives rise to four excitation branches. As discussed in Ref. 9 only two of the branches are visible at a time, in neutron scans along (*q* 0 0) or (0 0 *q*), allowing effectively the use of an extended zone scheme. The one-zone representation is obtained by folding the results in Figs. 6 and 7 with respect to *q*=1.5 producing the expected four branches per crystal-field level.

The two lowest branches, the *xx* excitations, show nearly no dispersion along *a*<sup>\*</sup> or *c*<sup>\*</sup>, but the two modes are bound to be strongly dispersive along *b*<sup>\*</sup>, where they, by symmetry, cross each other. This implies, in accord with the general considerations, that the directional average of the two branches obtained in the polycrystalline case only gives rise to a single level at about 2 meV. The experimental dispersion of the *yy*-polarized excitations is clearly different from the dispersion of the excitations polarized perpendicular to the *y* axis. In contrast to the constancy of the energies of the *xx* excitations, the energy difference between the two *yy* modes is small at (0 0 1) but becomes large at (0 0 2). This behavior shows that the exchange interaction is strongly anisotropic. Due to the polarization of the different modes, the *yy* excitations with energies close to 3.5 meV allow the determination of the *yy* component of the exchange interaction independently of the perpendicular components. Equivalently, the *xx* and *zz* components are determined by the ex-

TABLE III. The exchange parameters (in units of meV) derived from the experimental dispersion relations.  $\mathcal{J}^{\alpha\beta}(ij)$  is assumed to be diagonal with  $\mathcal{J}^{\alpha\alpha}(ij) = \mathcal{J}^{\alpha\alpha}(ij)$ . The first row shows the number of neighbors (*Z*) and the second the distances *d* between the ions.

	<i>I</i> <sub>1</sub>	<i>I</i> <sub>2</sub>	<i>I</i> <sub>3</sub>	<i>I</i> <sub>4</sub>	<i>I</i> <sub>5</sub>	<i>I</i> <sub>7</sub>
<i>Z</i>	2	2	2	2	4	4
<i>d</i> (Å)	3.76	3.78	4.52	5.14	5.56	5.97
$\mathcal{J}^{xx}(ij)$	0.0363	-0.0032	-0.0039	-0.0011	-0.0033	0
$\mathcal{J}^{yy}(ij)$	0.0174	0.0244	-0.0040	-0.0059	0.0042	-0.0046

citations with energies around 2 meV. The latter two components of the exchange interaction are assumed to be equal and the possible *xz* component is neglected. The values of the exchange parameters derived from the experimental excitation energies are given in Table III, and the comparisons between the calculated and experimental dispersion relations are shown in Figs. 6 and 7. The modes near the Bragg points are classified by *A*<sub>1</sub>–*A*<sub>4</sub> according to the scheme introduced in Ref. 9.

The parameters describing the exchange interaction between an ion on sublattice 1 and its neighbors are defined in Fig. 8. The coupling *I*<sub>6</sub> is neglected, but is effectively included in *I*<sub>2</sub> and *I*<sub>3</sub>. The parameter *I*<sub>3</sub>, which is the interaction between ions on the same sublattice lying a distance *b* from each other, is not really determined by the present experiments. A proper determination of this parameter would require a study of the dispersive effects along the *b* axis. Here, it plays the role of adjusting the effective crystal-field level spacing, i.e., the dominant effect of *I*<sub>3</sub> corresponds to a shift of the different positions of the three crystal-field levels in Table II by 0.02–0.05 meV. The resulting value of the ferromagnetic *xx* coupling of 0.043 meV is close to the value 0.023 meV suggested by the analysis of the susceptibility measurements [see Eq. (2)]. The ferromagnetic *yy* coupling

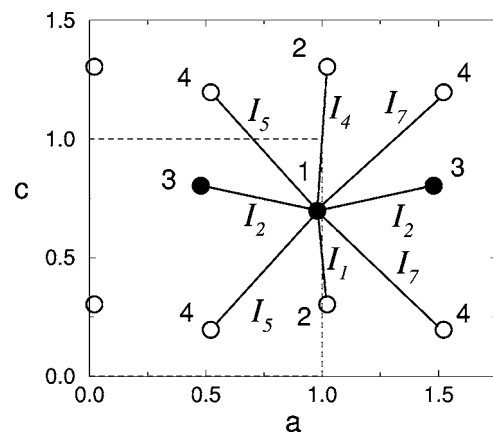


FIG. 8. The interactions  $I_p$  between ion 1 and its neighbors. The number *p* increases with the distance between the ions. *I*<sub>3</sub> is the coupling to the two ions on the same sublattice as 1 at the distance  $\pm b$ .

derived from Table III is  $\mathcal{J}_{yy}(\mathbf{0})=0.062$  meV, in comparison with the result of 0.113 meV derived from the fit to the susceptibility measurements, Eq. (2).

The dispersion along the  $c$  axis does not differentiate between the two coupling parameters  $I_5$  and  $I_7$ , describing the interactions between ions on sublattice 1 and 4 (or 2 and 3): only the sum  $I_5+I_7$  matters. When  $q$  is along the  $a$  axis, the difference  $I_5-I_7$  has some influence, but the few points available along this direction for the  $xz$  excitations leave the  $(xx,zz)$  component of this parameter undetermined. The effect of the  $yy$  component of  $I_5-I_7$  is relatively weak if considering the energies of the  $yy$  mode propagating along  $a$ . However, the comparison between the calculated and experimental intensity ratios of the two  $yy$  branches is improved substantially, when using  $I_7=-0.0046$  meV instead of 0. The intensities predicted by the final model agree in most details with the experimental data. One example is shown in Fig. 4 for the case of  $\mathbf{q}$  along the  $c$  axis. If the parameter  $I_7$  were neglected the upper branch of each of the three crystal-field excitations in Fig. 7 would be practically invisible in the  $(q\ 0\ 0)$  scans [or the  $(2-q\ 0\ 1)$  scan in the case of the longitudinal mode], whereas the introduction of  $I_7(yy)=-0.0046$ meV in the final model implies that the intensity ratio for the two  $yy$  modes is calculated to have a maximum value of about 0.7 at  $(1.6\ 0\ 0)$ . This is in agreement with experiments as shown in Fig. 5: notice that the upper branch is visible at  $(1.6\ 0\ 0)$ , but not at the equivalent  $(2.4\ 0\ 0)$  position.

At sufficiently low temperatures, the cooperative system of the electronic  $4f$  moments and nuclear spins of the Pr ions will order due to the hyperfine interaction. The lowest-energy mode is the  $xz$  mode with the symmetry  $A_3$  (antiferromagnetic along  $a$  and ferromagnetic along the  $c$  axis). The uncertainty about the value of  $I_3$  is of minor importance, and accepting the value of this parameter given in Table III, the energy minimum is 1.542 meV at  $(1\ 0\ 0)$ . The maximum of the  $xz$ -susceptibility tensor is found to occur along a direction making an angle of  $|\theta|=11.6^\circ$  with the  $x$  axis. The ordered phase is indicated by the arrows in Fig. 1 assuming  $\theta=+11.6^\circ$  for sublattices 1 and 2. This ordered phase is the same as observed in  $\text{HoF}_3$ , if we interchange the definition of the  $a$  and  $c$  axes in one of the systems. Accounting for the experimental value of  $\chi_{aa}$  in the zero-temperature limit, the value of the maximum component is estimated to be  $\sim 5.46+0.5$  meV $^{-1}$  in this limit. The effective coupling parameter is

$$\mathcal{J}(\theta) = 2(I_1 + I_3 + I_4) - \cos 2\theta(2I_2 + 4I_5 + 4I_7) \quad (3)$$

equal to 0.0806 meV. This leads to a critical ratio  $R_0 = \chi_{aa}(0)\mathcal{J}(\theta) \approx 0.48$ , and, including the hyperfine interaction, the ordering temperature of PrNiSn is estimated to be about 6 mK.

#### IV. CONCLUSION

The single-crystal susceptibility measurements show that PrNiSn is a highly anisotropic magnetic system at low temperatures. Because of the low symmetry of the surroundings of the non-Kramers Pr ions, the  $J=4$  multiplet splits into nine singlets. The present singlet ground-state system has the remarkable property that the matrix elements of the angular-momentum operators, of either  $(J_x, J_z)$  or  $J_y$ , between the ground state and each of the eight excited states are nonzero and of comparable magnitudes. Due to this circumstance seven of the eight excited levels were detected in the polycrystalline spectrum. The remaining level is estimated to lie at about 40 meV, just outside the range of the present experiments. The low symmetry of the Pr sites has the consequence that the crystal-field Hamiltonian contains 15 different parameters. The large number of parameters makes it impossible to guarantee that the set of CF parameters derived from the single-ion properties of the system is unique, but, as argued, the set derived should be useful for most practical purposes, one of which is the analysis of the magnetic excitations in the lower part of the spectrum.

The dispersion of the three lowest excited crystal-field levels has been measured along the symmetry directions of single-crystalline PrNiSn. The excitation spectrum is satisfactorily described in terms of the CF Hamiltonian and the neighboring coupling parameters. The analysis shows that the exchange interaction is relatively long ranged, extending out to the seventh nearest neighbors. The other important result is that the exchange interaction is anisotropic, as reflected in a dispersion of the  $yy$  mode that differs considerably from the dispersion of the  $xz$ -polarized modes. We finally conclude that the mean-field RPA model derived accounts in a satisfactory and coherent way for the comprehensive experimental observations made on PrNiSn.

#### ACKNOWLEDGMENTS

The experiments at ISIS were supported by the EPSRC and CCLRC of the U.K. The experiments at BENSIC were supported by the EU Access to Research Infrastructures programme. E.D.B. and J.P.A. thank EPSRC for the provision of financial support.

<sup>1</sup>T. Takabatake, F. Teshima, H. Fujii, S. Nishigori, T. Suzuki, T. Fujita, Y. Yamaguchi, J. Sakurai, and D. Jaccard, Phys. Rev. B **41**, 9607 (1990).

<sup>2</sup>D. T. Adroja, B. D. Rainford, and T. Takabatake, Physica B **253**, 269 (1998).

<sup>3</sup>Y. Andoh, M. Kurisu, S. Kawano, and I. Oguro, J. Magn. Magn.

Mater. **177-181**, 1063 (1998).

<sup>4</sup>S. Kawano, Y. Andoh, and M. Kurisu, J. Magn. Magn. Mater. **182**, 393 (1998).

<sup>5</sup>Ch. D. Routsis, J. K. Yakinthos, and H. Gamari-Seale, J. Magn. Magn. Mater. **117**, 79 (1992).

<sup>6</sup>M. Kurisu, R. Hara, G. Nakamoto, Y. Andoh, S. Kawano, and D.

- Schmitt, *Physica B* **312-313**, 861 (2002).
- <sup>7</sup>E. D. Beirne and K. A. McEwen (unpublished).
- <sup>8</sup>E. D. Beirne, K. A. McEwen, K. Habicht, and D. Fort, *Appl. Phys. A: Mater. Sci. Process.* **74** (Suppl.), S910 (2002).
- <sup>9</sup>M. J. M. Leask, M. R. Wells, R. C. C. Ward, S. M. Hayden, and J. Jensen, *J. Phys.: Condens. Matter* **6**, 505 (1994).
- <sup>10</sup>A. P. Ramirez and J. Jensen, *J. Phys.: Condens. Matter* **6**, L215 (1994).
- <sup>11</sup>J. Jensen, *Phys. Rev. B* **49**, 11833 (1994).
- <sup>12</sup>J. Jensen and A. R. Mackintosh, *Rare Earth Magnetism: Structures and Excitations* (Clarendon Press, Oxford, 1991).